Solvent Extraction Research and Development, Japan, **Vol. 33, No 1, 1 – 17 (2026)**

Environmentally Friendly Extraction of Novel Deep Eutectic Solvent for Gold Extraction

Zakiah D. NURFAJRIN[1], Adroit T. N. FAJAR[2], Mayu KAMISONO[1], Kevin SEPTIOGA[1] and Masahiro GOTO[1,*]

[1]*Department of Applied Chemistry, Graduate School of Engineering, Kyushu University, 744 Motooka, Fukuoka 819-0395, Japan;* [2]*Center for Energy Systems Design (CESD), International Institute for Carbon-Neutral Energy Research (WPI-I2CNER), Kyushu University, 744 Motooka, Fukuoka 819-0395, Japan*

** Corresponding author: m-goto@mail.cstm.kyushu-u.ac.jp*

(Received May 2, 2025; Accepted June 7, 2025)

Current industrial gold extraction processes primarily rely on toxic solvents and additives, which, despite their high efficiency, pose significant environmental and health hazards. Developing greener and more sustainable alternatives is therefore essential. Deep eutectic solvents (DESs) have recently gained attention as promising green solvents due to their tunable physicochemical properties and potential for selective metal extraction. In this study, we introduce a novel type V DES composed of *N*,*N*-diethylbenzamide (DEBA) and thymol (Thy), designed using COSMO-RS-predicted solid–liquid equilibrium phase diagrams to ensure eutectic behavior. DEBA-Thy demonstrated outstanding selectivity for Au^{3+} across a broad concentration range, achieving extraction efficiencies above 97%, while those of Pt^{4+} and Pd^{2+} remained below 10%. Slope analysis indicated a 1:1 stoichiometry for the Au(DES) complex. Additionally, cytotoxicity testing showed an EC_{50} value of 72.09 μmol/L, suggesting lower toxicity compared to conventional solvents. These findings support DEBA-Thy as a promising, sustainable solvent for selective gold recovery.

1. Introduction

Green chemistry has reshaped the way scientists approach chemical processes. Since Anastas and Warner [1] introduced the 12 principles of green chemistry, there has been a concerted global effort to develop sustainable alternatives that minimize hazardous waste [1-4]. According to Martins et al. [5], deep eutectic solvents (DESs) are eutectic mixtures of a hydrogen bond acceptor (HBA) and a hydrogen bond donor (HBD) that are stable in the liquid phase even when their eutectic temperatures are lower than those of their individual components. In addition, DESs have emerged as promising candidates due to their low toxicity, biodegradability, ease of synthesis, availability, and cost-effectiveness [6].

The increasing demand for precious metals has led to their recovery from various secondary resources, such as electronic waste, spent catalysts, and permanent magnets [7-10]. Their co-occurrence in these materials presents both an opportunity and a challenge for resource recovery [11-17]. DESs have emerged as promising green alternatives to conventional solvents due to their ability to undergo specific interactions with various metal ions, which makes them suitable candidates for multi-metal extraction systems [11-13]. However, the application of DESs in gold extraction is limited, with few studies available. Khuduwe *et al.* [14] used ethaline (choline chloride and ethylene glycol) to leach gold from tailings, achieving a 71.9%

extraction efficiency with significantly higher than that for conventional cyanidation (46.9%). In addition, several studies on ethaline DESs have used additives such as Aliquat 336 [15], copper(II) chloride dihydrate [16], and tetra(2-ethylhexyl)malonamide [15] to enhance selectivity and performance. While these additives can improve extraction efficiency, they may also introduce toxicity concerns [17], potentially compromising the environmental benefits that DESs offer.

Therefore, DES-based gold extraction methods are essential to develop and maintain the characteristics of a green solvent while achieving high extraction efficiency. Since DESs are mixtures of two or more components, solid–liquid equilibrium (SLE) phase diagram data are essential to determine the eutectic temperature, which is a key criterion for DES formation. However, designing new DESs through experimental methods would be labor-intensive, costly, and time-consuming due to the large number of possible component combinations [18,19]. To address this challenge, computational methods, particularly quantum chemistry calculations, have become invaluable tools in accelerating solvent discovery before considering their application in liquid−liquid extraction processes [20].

Beyond functional performance, ensuring the environmental and health safety of DESs is equally important. A solvent that is effective but poses toxicity risks would contradict the principles of green chemistry. Cytotoxicity analysis plays a crucial role in evaluating the biocompatibility of DESs, ensuring they meet environmental and safety standards before large-scale adoption. Atashnezhad *et al.* [21] conducted cytotoxicity tests on selected DESs using the HEK-293 cell line. Furthermore, Ahmadi *et al.* [22] evaluated the cytotoxicity of choline chloride-based DESs, confirming their safety for use in pharmaceutical and environmental applications. By incorporating cytotoxicity evaluations into our study, we believe that the selected DESs are both effective and safe for practical applications.

In this study, we designed a new green hydrophobic DES with high selectivity for Au^{3+}, presenting a comprehensive framework for the accelerated discovery of sustainable DESs for metal extraction. This framework integrates computational chemistry with experimental validation through extraction performance and cytotoxicity analysis. First, we identified nine HBAs and nine HBDs based on their potential to effectively coordinate with gold ions. Second, we evaluated 81 DES combinations using SLE phase diagrams to identify candidates with suitable eutectic temperatures (T_e). Third, we synthesized the selected DESs and screened them based on their SLE phase diagram behavior and viscosity below 100 mPa·s, an important criterion for industrial applicability [19]. Fourth, we performed gold extraction experiments to assess the selectivity and efficiency of the selected DESs. Finally, to ensure environmental safety, we conducted cytotoxicity analysis using the HEK-293 cell line. This approach offers both high performance and sustainability, aligning with the core principles of green chemistry and demonstrating potential for industrial application.

2. Methods

2.1 DFT and COSMO-RS

The Conductor-like Screening Model for Real Solvents (COSMO-RS) is a molecular modeling approach that combines quantum chemistry and statistical thermodynamics to predict SLE phase diagrams for solvents [23,24]. We began by designing the three-dimensional (3D) molecular structures of HBAs and HBDs using TURBOMOLE software (TmoleX version 4.5). These structures were generated by inputting

their Simplified Molecular Input Line Entry Specification (SMILES) representations into the software. Subsequently, geometry optimization was performed at the density functional theory (DFT) level using the def-TZVP (triple-ζ valence polarized) basis set and the generalized gradient approximation Becke–Perdew (GGA-BP86) exchange–correlation functional [25,26]. To ensure numerical accuracy, the self-consistent field density convergence threshold was set to 1×10^{-6} Ha. The optimized molecular structures were then exported as COSMO files from TURBOMOLE and imported into the COSMOthermX tool for further analysis. All calculated SLE phase diagrams have been deposited at the following link: [https://doi.org/10.6084/m9.figshare.29146451.v1].

2.2 Materials

Lidocaine (purity 99%), choline chloride, and vanillin were purchased from Wako Pure Chemical (Osaka, Japan). *N*,*N*-diethylbenzamide (DEBA; purity 99%), 1,8-cineole, diethanolamine, phenol, 1,8-octanediol, imidazole, 2-naphthol, urea, acetamide, bis(2-pyridylmethyl)amine, histidine, L-serine, thymol (Thy), diethanolamine, HCl (5 and 10 mol/L), H_2SO_4 (5 mol/L), and dimethyl sulfoxide (DMSO) were purchased from Kishida Chemical (Osaka, Japan). Standard solutions of Au^{3+}, Pd^{2+}, and Pt^{4+} (1000 mg/L), toluene, and low-glucose Dulbecco's Modified Eagle Medium (D-MEM) were purchased from Wako Pure Chemical (Osaka, Japan). Fetal bovine serum (FBS) and antibiotic−antimycotic were purchased from Thermo Fisher Scientific (Waltham, MA). A WST-8 cell counting kit was purchased from Dojindo Molecular Technologies (Kumamoto, Japan), and the HEK-293 mammalian cell line was provided by the RIKEN Cell Bank (Tsukuba, Japan).

2.3 Preparation of selected DESs

The selected DESs were synthesized by combining HBAs and HBDs in molar ratios determined based on SLE phase diagrams generated from COSMO-RS calculations. The candidate HBAs and HBDs are presented in Table 1. Each DES was prepared by accurately weighing the HBA and HBD components using an analytical balance with a precision of ±0.1 mg. The components were mixed in a 10 mL glass bottle and heated with continuous magnetic stirring at temperatures ranging from 25 to 80 °C at 650 rpm, depending on the melting points of the individual components, until a homogeneous and transparent liquid was formed. The heating duration varied between 15 min and 2 h, ensuring complete dissolution and interaction between the components [27,28]. Upon achieving a uniform liquid, the mixture was allowed to cool to room temperature under ambient conditions. No additional purification steps were necessary, as the synthesis process did not involve any side reactions or by-products [29].

2.4 Density and viscosity measurement

The density of the selected DESs was measured using a DMA 35 Version 4 digital density meter (Anton Paar GmbH, Graz, Austria), while viscosity was determined using a Lovis/ME 2000 viscometer from the same manufacturer. All measurements were performed at a controlled temperature to ensure consistency and minimize external influences.

2.5 Hydrophobicity test

The hydrophobicity test was performed by mixing each DES with water in a 1:1 volume ratio inside a polypropylene tube, using vortex mixing to achieve equilibrium at room temperature (298.15 K). The mixture was then centrifuged at 10,000 g for 2 min at the same temperature to separate the organic and aqueous phases.

Table 1. Candidate HBAs and HBDs.

HBA	Chelating agent to metal	HBD	Chelating agent to metal
Lidocaine	Amide (-CONH-), Tertiary Amine ($-N(CH_3)_2$)	Vanillin	Hydroxyl (-OH), Aldehyde (-CHO), Ether ($-OCH_3$)
N,*N*-Diethylbenzamide	Amide (-CONH-), Aromatic ring	Thymol	Hydroxyl (-OH), Isopropyl ($-C_3H_7$)
Acetylcholine chloride	Ester (-COO-), Quaternary Ammonium ($-N^+(CH_3)_3$)	Diethanolamine	Secondary Amine (-NH), Two Hydroxyl (-OH)
1,8-Cinole	Ether (-O-)	Phenol	Hydroxyl (-OH)
Acetamide	Amide ($-CONH_2$)	1,8-Octanediol	Two Hydroxyl (-OH)
Bis(2-pyridylmethyl) amine	Two Pyridine ($-C_5H_5N$) Rings, Amine (-NH-)	Imidazole	five-membered aromatic heterocycle containing two nitrogen atoms
Choline chloride	Hydroxyl (-OH), Quaternary Ammonium ($-N^+(CH_3)_3$)	2-Naphthol	A hydroxyl (-OH) group at position 2
Histidine	Amino ($-NH_2$), Carboxyl ($-COO^-$), Imidazole ($-C_3N_2H_4$)	Thiourea	Thione (-C=S), Amine ($-NH_2$)
L-Serine	Amino ($-NH_2$), Carboxyl ($-COO^-$), Hydroxyl (-OH)	Urea	Amide ($-CONH_2$)

2.6 ^{1}H NMR and FTIR analysis

The synthesized DESs were characterized using proton nuclear magnetic resonance (^{1}H NMR) spectroscopy (ECZ400S, JEOL, Tokyo, Japan) and Fourier-transform infrared (FTIR) spectroscopy (Spectrum Two, PerkinElmer, Waltham, MA, USA). FTIR spectra were recorded over the range of 500–4000 cm^{-1}, accumulating four scans per sample to analyze intermolecular interactions.

The ^{1}H NMR measurements were conducted with 64 scans per sample. Chemical shifts were referenced to the residual proton signals of the deuterated solvents: 4.79 ppm for D_2O, 7.26 ppm for $CDCl_3$, and 2.50 ppm for DMSO-d_6 [30,31]. The deuterated solvents [32] used for sample preparation were selected based on the solubility of the DES components:

a) D_2O for lidocaine–vanillin
b) D_2O for acetylcholine chloride–diethanolamine.
c) $CDCl_3$ for DEBA-Thy.
d) DMSO-d_6 for choline acetate.

2.7 DSC analysis

The thermal behavior of the synthesized DESs was evaluated using a differential scanning calorimeter (DSC) (XDSC-7000, HITACHI, Ibaraki, Japan). Approximately 10 mg of each sample was accurately weighed and hermetically sealed in an aluminum pan to prevent moisture absorption and contamination.

The DSC measurements were conducted to investigate the melting and solid–liquid phase transitions

of the DESs, guided by eutectic temperatures predicted from COSMO-RS SLE phase diagrams. The temperature program consisted of the following steps:

a) Cooling from 30 °C to 0 °C
b) Further cooling from 0 °C to −80 °C
c) Heating from −80 °C to 0 °C
d) Final heating from 0 °C to 30 °C

Each heating and cooling segment was performed at a rate of 5 °C/min. A dry nitrogen purge gas was employed throughout the DSC analysis to maintain an inert atmosphere and prevent oxidative degradation. The nitrogen purge was maintained at a flow rate of 50 mL/min and a pressure between 100 and 140 kPa gauge (15–20 psig), consistent with standard DSC operating conditions.

2.8 Metal extraction

Aqueous metal solutions containing 5, 50, and 150 mg/L of Au^{3+}, Pd^{2+}, and Pt^{4+} were prepared from their respective 1000 mg/L standard solutions and adjusted to discrete pH values of 1, 3, and 5 using HCl and H_2SO_4. The pH was measured with a pH meter (HM-30R, DKK-TOA, Tokyo, Japan). The volume ratios of organic to aqueous phases (O/A) were varied systematically as 1:1, 1:2, 1:3, 1:5, 1:7, 1:8, 1:10, 1:15, and 1:20 to identify the optimum extraction conditions. All experiments were conducted in 15 mL polypropylene tubes with a total working volume of 10 mL. The tubes were mechanically shaken at 160 rpm for 5 min to 6 h at room temperature (298.15 K), followed by centrifugation (TOMY SEIKO Co., Ltd., Tokyo, Japan) with a 21 mm rotor at 10,000 g for 5 min to separate the two phases. The organic layer was carefully separated, and the metal concentrations in the aqueous phase were measured using an inductively coupled plasma optical emission spectrometer (Optima 8300, PerkinElmer Co., Waltham, MA). The extraction efficiency (%E) and distribution ratio (D) were calculated as follows:

$$\%E = \frac{[\mathrm{M}]_{\mathrm{init}} - [\mathrm{M}]_{\mathrm{eq}}}{[\mathrm{M}]_{\mathrm{init}}} \times 100\% \quad (1)$$

$$D = \frac{[\mathrm{M}]_{\mathrm{init}} - [\mathrm{M}]_{\mathrm{eq}}}{[\mathrm{M}]_{\mathrm{eq}}} \quad (2)$$

where $[\mathrm{M}]_{\mathrm{init}}$ and $[\mathrm{M}]_{\mathrm{eq}}$ represent the concentrations of metal ions before and after extraction, respectively.

2.9 *In vitro* cytotoxicity assay

The *in vitro* cytotoxicity of selected DESs was assessed using the HEK-293 cell line [21]. HEK-293 cells in D-MEM medium (D-MEM containing 10% (v/v) FBS and 1% (v/v) antibiotic–antimycotic) were seeded at a density of 5,000 cells per well in a 96-well plate (Greiner Bio-One GmbH) and incubated in a CO_2 incubator at 37°C for 24 h. The culture medium was then supplemented with DESs at varying concentrations in reduced serum medium (OPTI-MEM). Cells were exposed to the treatment for 24 h, after which the medium was removed, and the cells were washed with Dulbecco's Phosphate-Buffered Saline (D-PBS) (Nacalai Tesque, Inc., Kyoto, Japan). Subsequently, 100 µL of WST-8 [33] cell counting kit solution (Dojindo Molecular Technologies, Inc., Rockville, MD, USA) in OPTI-MEM was added to each well, followed by incubation for 3 h at 37°C. The absorbance of WST-8 formazan was measured at 450 nm using a microplate reader (Bio-Tek Instruments, Inc., Winooski, VT, USA). Untreated cells maintained under

identical conditions served as controls. Cell viability was calculated using eq. (3).

$$\text{Cell viability}(\%) = \left(\frac{A_{\text{test}} - A_{\text{blank}}}{A_{\text{control}} - A_{\text{blank}}} \right) \times 100\% \quad (3)$$

where A_{test}, A_{control}, and A_{blank} correspond to the absorbance values of the wells containing DESs, the solvent control (0.5% v/v ethanol or 0.5% v/v DMSO), and the solvent without HEK-293 cells, respectively. The half-maximal effective concentration and inhibitory concentration (EC_{50} and IC_{50}) [34] in solvent extraction for cytotoxicity evaluation have the same meaning and were calculated using Prism-GraphPad 6.0 (Dotmatics, Boston, MA) based on eq. (4) [34]. The average of the estimates of the minimum (a) and maximum (d) equals the 50% response, that is, the relative EC_{50} or IC_{50}. The steepness of the linear portion of the curve is described by the slope factor b, and the parameter c is the concentration corresponding to the response midway between a and d.

$$EC_{50} \text{ or } IC_{50} = c \left(\frac{a - 50\% \text{ response}}{50\% \text{ response} - d} \right)^{\frac{1}{b}} \quad (4)$$

3. Results and Discussion

3.1 Screening DES combinations using SLE phase diagrams

We first performed a screening process to identify novel DESs using COSMO-RS calculations to

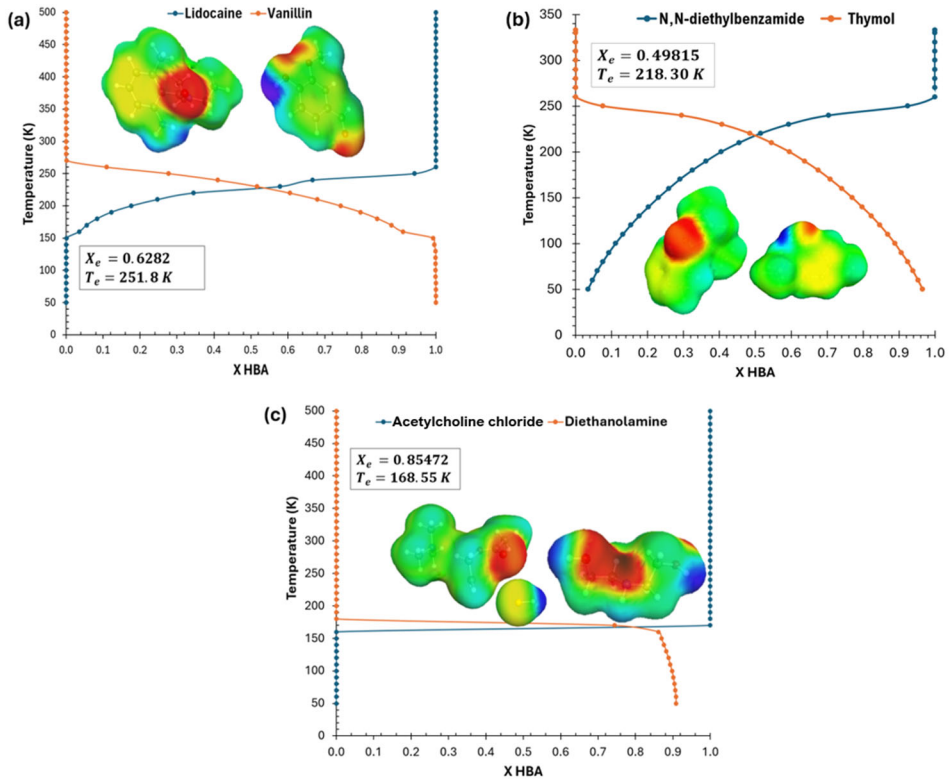

Figure 1. SLE-phase diagrams of (a) lidocaine–vanillin (Lid-Van), (b) *N*,*N*-Diethylbenzamide–thymol (DEBA-Thy), and (c) acetylcholine chloride–diethanolamine (AChCl-DEA).

evaluate the eutectic temperatures of 81 HBA–HBD combinations. For the complete SLE phase diagrams for all combinations, please refer to Section 2.1. Figure 1(a–c) presents the screening results. The mixtures with eutectic temperatures T_e (representing the melting temperature (T_m)) below 298.15 K include acetylcholine chloride–diethanolamine (AChCl-DEA), shown in Figure 1(c), which reached a T_e of 168.55 K with a eutectic mole fraction (x_e) of 0.85472. In contrast, the DES formed by lidocaine–vanillin (Lid-Van) (Figure 1(a)) exhibited T_e of 251.8 K with x_e of 0.6282, while the DES of DEBA-Thy (Figure 1(b)) showed a similar T_e of 281.3 K and x_e of 0.49815. Figure 1(a–c) also illustrates the 3D structures of the HBAs and HBDs in each DES. Additionally, the activity coefficients (ln(γ)) of Lid-Van, DEBA-Thy, and AChCl-DEA are –21.99, –184.35, and –41.19, respectively, further confirming the intermolecular interactions between the HBA and HBD in the DES system.

To validate the predicted melting temperatures of the selected DESs, we also conducted experimental measurements using DSC. The predicted and experimental values of T_m were in good agreement, as shown in Table 2. For Lid-Van, the difference between the predicted and measured melting temperatures was 0.76 K. In contrast, DEBA-Thy exhibited a larger difference of 4.15 K. For AChCl-DEA, the predicted melting temperature was 168.55 K, while the experimental value was expected to be below 193.5 K due to the lower detection limit of the DSC measurement method.

Table 2. Comparison of melting temperature of selected DESs between prediction and experiment results.

Selected of DES		**T_m by Prediction (K)**	**T_m by Experiment (K)**
HBA	**HBD**		
Lidocaine	Vanillin	245.94	245.18
N,*N*-Diethylbenzamide	Thymol	218.30	214.15
Acetylcholine Chloride	Diethanolamine	168.55	<193.15

3.2 Synthesis of DESs

As a validation step following the eutectic temperature predictions by COSMO-RS, we synthesized 81 DES candidates. Among them, only three formed a stable liquid phase at 298.15 K. Table 3 shows the results of hydrophobicity tests for mixtures 1–3 to determine their suitability for the metal extraction method (Figure 2(a–f)). The DESs Lid-Van and AChCl-DEA formed a stable, immiscible phase when mixed with aqueous metal solutions. In contrast, DEBA-Thy exhibits two-phase formation behavior. Furthermore, the intermolecular interactions were confirmed by comparing the FTIR and ^{1}H NMR spectra of the DES, HBA, and HBD compounds, as shown in Figures 3 and 4, respectively.

Table 3. Screening results of Mixtures HBA/HBD by COSMO-RS at their phases in room temperature

Selected of DES		**Phase at 298.15 K**	**Molar fraction**	**Hydrophobicity**	**Temperature synthesis (K)**
HBA	**HBD**				
Lidocaine	Vanillin	Liquid	2.1:1	Immiscible formation	378.15
N,*N*-Diethylbenzamide	Thymol	Liquid	1:1	Two phase formation	300.15
Acetylcholine Chloride	Diethanolamine	Liquid	6:1	Immiscible formation	318.15

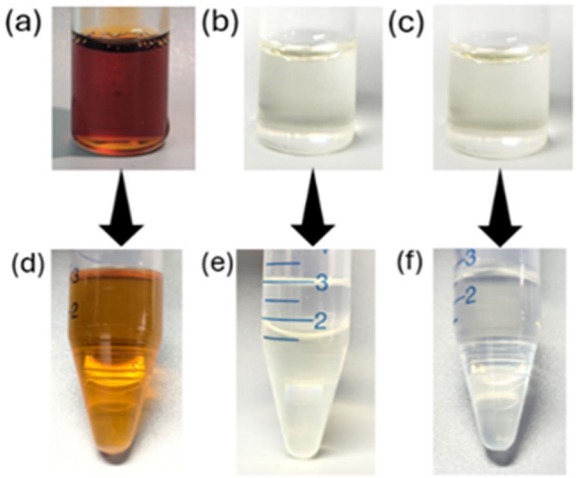

Figure 2. Photographs of the synthesized DESs: (a) Lid-Van, (b) DEBA-Thy, and (c) AChCl-DEA, along with hydrophobic/hydrophilic behaviour tests of the DESs:
(d) Lid-Van, (e) DEBA-Thy, and (f) AChCl-DEA.

The formation of Lid-Van was also confirmed by FTIR spectroscopy (Figure 3(a)). Notable spectral shifts indicate hydrogen bond formation between the constituent molecules. The N–H stretching vibrations of lidocaine, originally observed at 3,451 and 3,385 cm^{-1}, exhibit both shifts and intensity variations in the DES spectrum, confirming intermolecular interactions. Additionally, the aldehyde C–H stretching band of vanillin, typically appearing at 2,727 cm^{-1}, undergoes modifications, suggesting interactions with lidocaine. Further evidence is provided by alterations in the C=O stretching peak of lidocaine at 1,655 cm^{-1}, which further confirms the presence of strong hydrogen bonding within the DES structure.

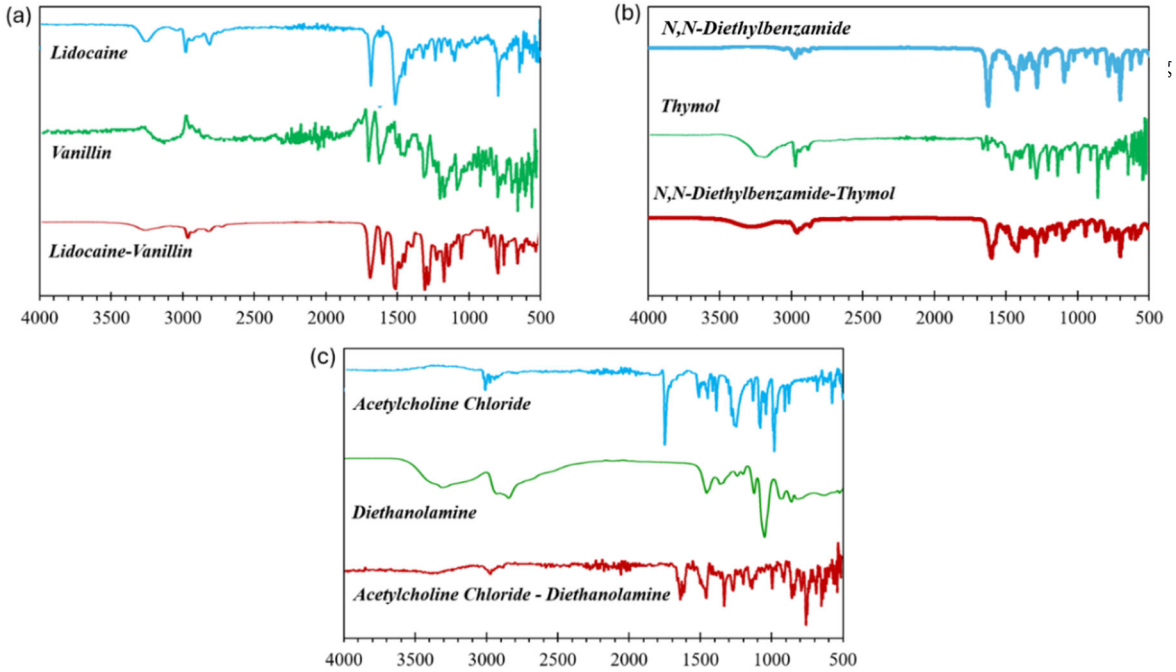

Figure 3. Comparison of FTIR spectra of (a) Lid-Van, (b) DEBA-Thy, and (c) AChCl-DEA.

In addition, the formation of DEBA-Thy was validated through FTIR analysis (Figure 3(b)). The O–H stretching band of Thy, detected in the range of 3,200–3,500 cm^{-1}, exhibits broadening and shifting in the DES spectrum, indicative of hydrogen bond formation with DEBA. Additionally, the C=O stretching vibration of DEBA, initially observed at 1,645 cm^{-1}, shows modifications in intensity and position, further supporting molecular interactions. The appearance of new spectral features and shifts in the DES spectrum confirm the successful formation of a stable eutectic mixture through hydrogen bonding.

Moreover, AChCl-DEA (Figure 3(c)) also confirms strong hydrogen-bonding interactions between its components. The individual spectra of acetylcholine chloride and diethanolamine show characteristic O–H and N–H stretching vibrations within 3,200–3,500 cm^{-1}, along with C–O and C–N stretching vibrations within 1,000–1,500 cm^{-1}. Significant broadening and shifting in the O–H and N–H regions upon DES formation indicate enhanced hydrogen bonding, while alterations in C–O and C–N vibrations suggest structural reorganization within the DES network.

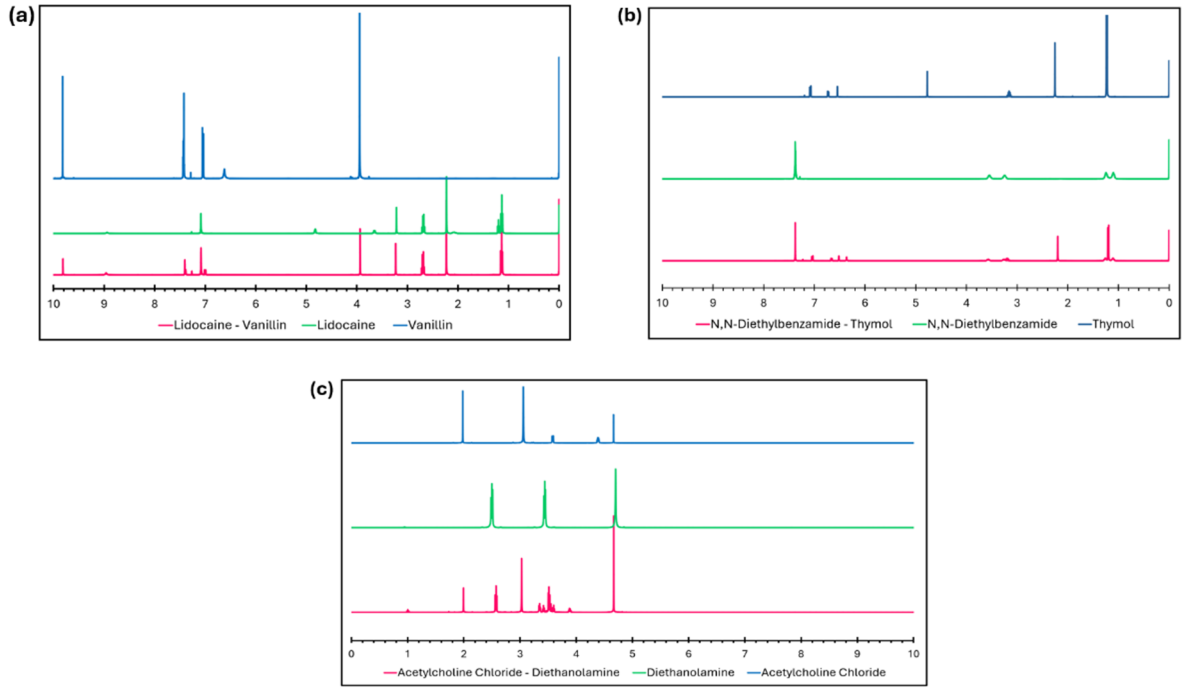

Figure 4. Comparison of ^{1}H NMR spectra of selected DESs using chloroform-d, DMSO-d_6, and D_2O.

The ^{1}H NMR spectra (400 MHz, $CDCl_3$, DMSO-d_6, and D_2O) confirm the formation of DES through chemical peak shifts and broadening, indicating strong intermolecular interactions. For DEBA-Thy (Figure 4(a)), the hydroxyl (-OH) proton of Thy (δ 4.77) shifts significantly, suggesting hydrogen bonding with the carbonyl (C=O) group of the HBA. Aromatic protons (δ 6.5–7.4) show downfield shifts and broadening, indicating π–π (aromatic ring stacking) interactions, while methylene (-CH_2) and methyl (-CH_3) groups show slight shifts, supporting dipole–dipole interactions.

In Lid-Van (Figure 4(b)), the aldehyde proton of vanillin (δ 9.81) broadens and shifts downfield due to hydrogen bonding with the amide (-NH) group of lidocaine. Aromatic signals (δ 7.0–7.4) shift and broaden, suggesting π–π interactions, while the methoxy (-OCH_3) and aliphatic (-CH_3) groups show slight reductions

in electron density, confirming dipole–dipole interactions. Furthermore, for AChCl-DEA (Figure 4(c)), the downfield shift of methylene (-CH_2) protons (δ 3.90–3.32) and the broadening of peaks at δ 4.67 and δ 3.61 indicate hydrogen bonding and ionic interactions between the quaternary ammonium (-N^+CH_3) group of acetylcholine chloride and the hydroxyl (-OH) groups of diethanolamine. Downfield shifts at δ 1.99 and δ 1.73 further support the stabilization of the DES through hydrogen bonding and electrostatic interactions.

3.3 Characterization of selected DESs

The density of a mixture is primarily governed by two factors, the molecular packing of its constituent components and the intermolecular interactions among them [35]. As shown in Table 4, the densities of the synthesized DESs span a relatively wide range (0.990–1.222 g/cm^3). From a solvent design perspective, this variability is advantageous, offering greater flexibility in selecting solvents tailored to specific application requirements. In ionic-based DESs, an increase in the cation alkyl chain length typically leads to a decrease in density, as illustrated by the AChCl-DEA system. Additionally, the length of the HBD chain significantly affects the density of DESs [36]. DESs with longer HBD chains, such as DEBA-Thy, tend to exhibit lower densities, whereas those with shorter chains, such as Lid-Van, generally show higher densities, as confirmed by our experimental measurements. This trend aligns with the general observation that longer alkyl chains in HBD components create a more loosely packed molecular structure, thereby reducing the overall density.

Viscosity plays a crucial role in determining the practical applicability of DESs in industrial liquid–liquid extraction systems. High-viscosity solvents often inhibit mass transfer, slow down extraction kinetics, and increase energy consumption during pumping and processing [37-40]. The viscosity of the synthesized DEBA-Thy DES was measured to be 37.7 mPa·s at 298.15 K; previous studies suggest that DESs with viscosities below 100 mPa·s are generally considered suitable for industrial applications due to their improved handling and operational efficiency [19,37,38]. The relatively low viscosity of DEBA-Thy enhances metal ion transport and promotes efficient phase separation, both of which are essential for optimizing continuous-flow extraction systems.

Table 4. Density and Viscosity of DES

DESs	Density (g/cm^3)	Viscosity (mPa·s)
Lid-Van	1.099	2049
DEBA-Thy	0.9905	37.7
AChCl-DEA	1.2223	369.4

3.4 Metal extraction

Figure 5 illustrates the effect of the O/A phase ratio on the extraction efficiency (%*E*) of Au^{3+}, Pt^{4+}, and Pd^{2+} using the hydrophobic DEBA-Thy DES for different acid types using H_2SO_4 (Figure 5(a)-(c)) and HCl (Figure 5(d)-(f)) at pH values of 1, 3, and 5. As shown in Figure 5, the O/A phase ratio of 1:5 yielded the best extraction performance and was therefore adopted for subsequent experiments. Notably, the extraction efficiency of Au^{3+} reached 97% in H_2SO_4 and 92.8% in HCl after 2 h of contact time, with distribution ratios (*D*) exceeding 200, demonstrating the high affinity of gold ions at DEBA-Thy under these conditions.

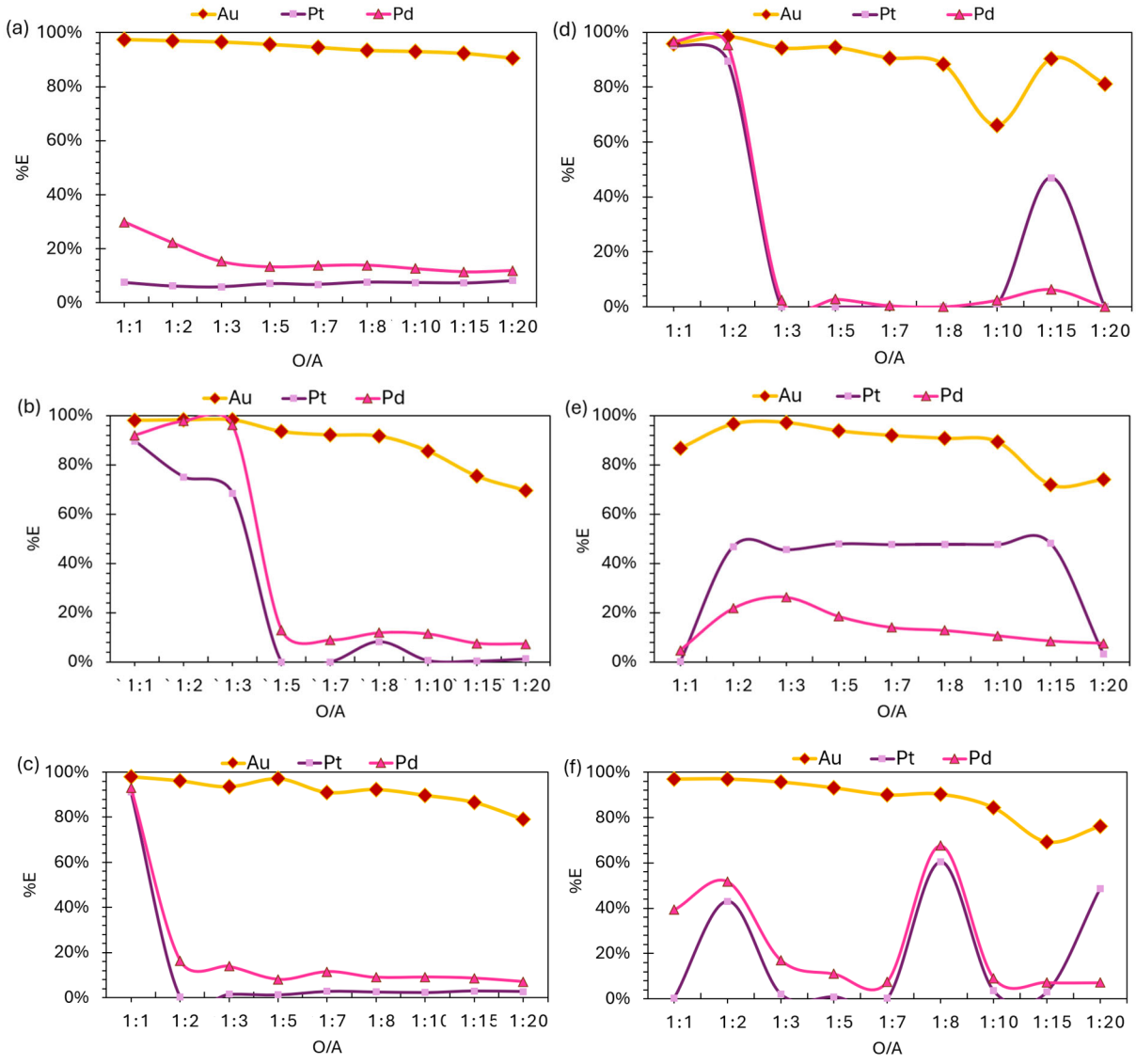

Figure 5. Effect of O/A on extraction efficiency for each pH and acid after 2 h (5 ppm metal solution): (a) H_2SO_4, pH 1, (b) H_2SO_4, pH 3, (c) H_2SO_4, pH 5, (d) HCl, pH 1, (e) HCl, pH 3, and (f) HCl, pH 5.

Furthermore, the effect of acid strength on extraction efficiency was examined using H_2SO_4 at pH values of 1, 3, and 5, as shown in Figure 6. Gold extraction efficiencies were consistently high across all pH levels, with the highest selectivity (97.01%) observed at pH 5, indicating effective coordination of Au^{3+} ions even under mildly acidic conditions. In contrast, the extraction efficiencies of Pt^{4+} and Pd^{2+} remained considerably lower than that of Au^{3+} under all pH conditions. This trend highlights the effectiveness of pH control using H_2SO_4 for selective gold extraction and is further supported by the markedly higher distribution ratio of Au^{3+} (D > 370 at pH 1), suggesting that the sulfate medium promotes favorable coordination and enhances the solubility of metal–DES complexes [41].

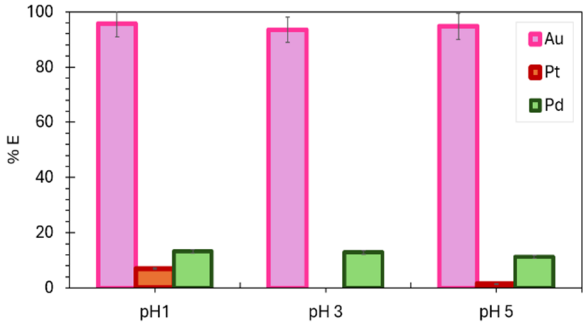

Figure 6. Effect of H_2SO_4 pH on extraction efficiency (%*E*) of Au^{3+}, Pt^{4+}, and Pd^{2+} (O/A ratio = 1:5, *T* = 298.15 K).

Figure 7 illustrates the extraction efficiency (%*E*) of Au^{3+}, Pt^{4+}, and Pd^{2+} from aqueous solutions using DEBA-Thy under mild conditions (O/A = 1:5, pH 5, 5 ppm metal)). Au^{3+} demonstrated exceptional extraction performance, achieving over 95.68% efficiency in just 5 min and maintaining a consistent extraction efficiency of 97.33% throughout the 6-h duration. This rapid and sustained extraction of Au^{3+} indicates a strong affinity between gold ions and DEBA-Thy, likely facilitated by coordination with the amide carbonyl group and possible π–π interactions involving the aromatic rings of both DEBA and Thy.

In contrast, the extraction efficiencies for Pd^{2+} were markedly lower, reaching only about 12% even after extended contact times. Pt^{4+} exhibited the least affinity for the DES, with extraction efficiencies consistently below 2% throughout the experiment. These findings underscore the pronounced selectivity of DEBA-Thy for Au^{3+} over Pd^{2+} and Pt^{4+}, which is particularly advantageous for the selective recovery of gold from complex, multi-metal solutions. The distinct disparity in extraction efficiencies highlights the crucial influence of the DES's chemical structure and the unique coordination chemistry of Au^{3+} ions.

Figure 8 illustrates the extraction performances of Au^{3+}, Pt^{4+}, and Pd^{2+} using the DEBA-Thy system over a 4-h contact time at initial metal concentrations of (a) 50 ppm and (b) 150 ppm. At the lower concentration (Figure 8(a)), Au^{3+} demonstrated exceptional extraction efficiency, exceeding 95% throughout the duration, highlighting the DES's strong affinity and selectivity for gold even in mixed-metal solutions. Conversely, the Pt^{4+} and Pd^{2+} extraction efficiencies remained below 10%, indicating negligible interference and confirming the highly selective nature of the DEBA-Thy toward Au^{3+} under these conditions.

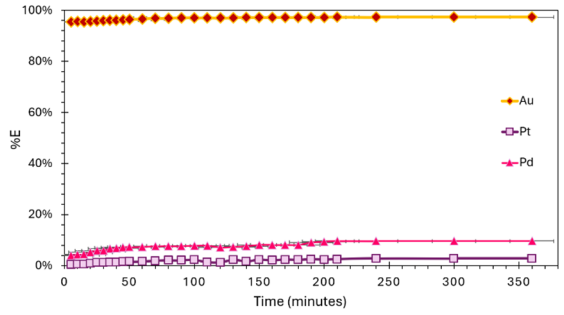

Figure 7. Extraction efficiency (%*E*) of Au^{3+}, Pd^{2+}, and Pt^{4+} using DEBA-Thy (O/A ratio of 1:5, H_2SO_4, pH 5, 2 h, 5 ppm metal, *T* = 298 K).

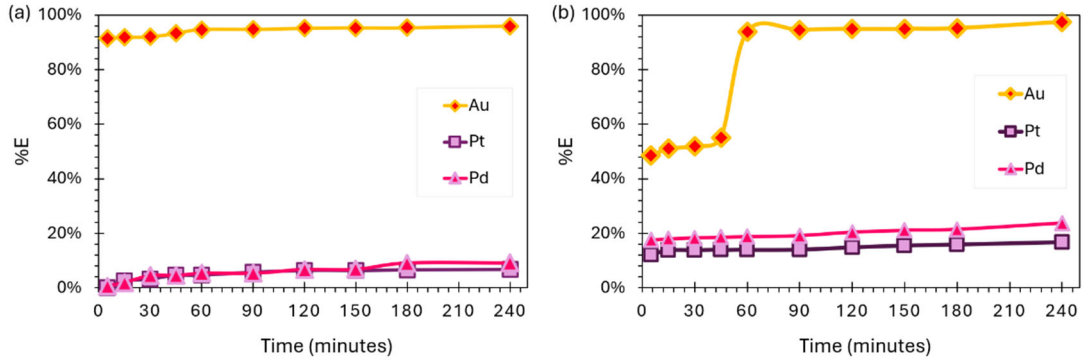

Figure 8. Extraction efficiency (%*E*) of Au^{3+}, Pd^{2+}, and Pt^{4+} using DEBA-Thy (O/A ratio of 1:5, H_2SO_4, pH 5, 2 h, T = 298 K), and (a) 50 ppm and (b) 150 ppm of metal solution.

When the initial metal concentration was increased to 150 ppm (Figure 8(b)), the Au^{3+} extraction efficiency remained above 90% despite the higher metal load. This demonstrates the robustness of the DES system in maintaining strong selectivity and extraction efficiency for Au^{3+} even under increased concentrations and potential competitive effects. Although the extraction efficiencies for Pt^{4+} and Pd^{2+} slightly increased (to up to 20%) at 150 ppm, likely due to improved mass transfer at elevated solute levels, the DES system still clearly preferentially coordinates and extracts Au^{3+} over these metals.

3.5 Extraction mechanism

To better understand the interaction between DEBA-Thy and gold ions during extraction, UV–Vis and FTIR spectroscopy analyses were conducted before and after the extraction process, in Figure 9(a) shown the shift of UV–Vis analysis indicates that the gold ion remains in its original chemical form but experiences a different local environment due to coordination with DES molecules. Collectively, these spectroscopic findings suggest that gold is selectively extracted into the DES phase primarily through non-covalent interactions, such as hydrogen bonding and ion pairing, without alteration of the gold complex's chemical structure. The characteristic absorbance peak of the gold ion, typically observed at 314 nm, exhibited a slight redshift to 318 nm after extraction into the DES.

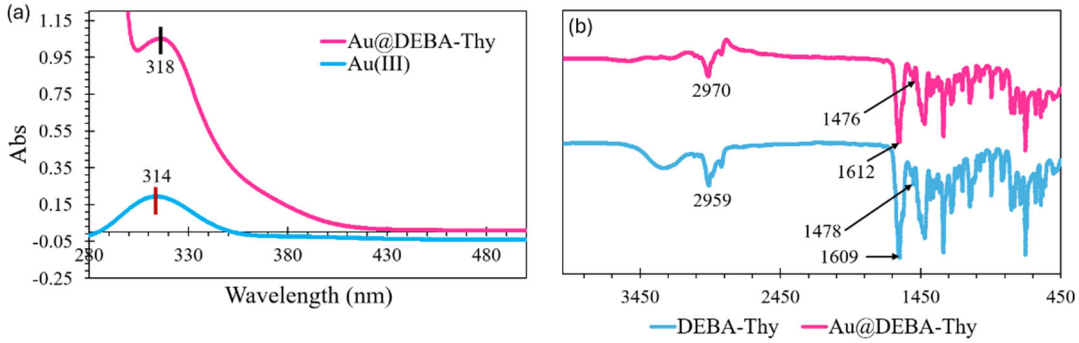

Figure 9. (a) UV-Vis spectra of Au(III) and Au@DEBA-Thy; (b) FTIR spectra of Thy-DEBA and Au@DEBA-Thy.

Furthermore, Figure 9(b), the FTIR spectra exhibit the C–H stretching vibration of the alkyl groups shifted from 2,959 to 2,970 cm^{-1}, indicating subtle changes in the local molecular environment due to

interaction with gold ions [42,43]. The amide C=O stretching band moved slightly from 1,609 to 1,612 cm^{-1}, suggesting weak coordination or hydrogen bonding between the DEBA-Thy and Au^{3+} ions [42,43]. Additionally, the aromatic ring vibration exhibited a minor shift from 1,478 to 1,476 cm^{-1}, which may reflect π-interactions or minor conformational changes within the DEBA-Thy structure following gold extraction [42,43]. Based on these experimental observations, the extraction mechanism likely proceeds via the following ion-association pathway [42,43].

$$[DES]_{(organic)} + H^{+}_{(aqueous)} + AuCl^{-}_{(aqueous)} \rightleftarrows [H(DES)][AuCl_4]_{(organic)} \quad (5)$$

Figure 10 presents the slope analysis for gold extraction using DEBA-Thy dissolved in toluene at pH 5 with a 2-h contact time. The plot of log D versus log[DEBA-Thy] concentration yielded a slope of approximately 0.9, indicating a near 1:1 stoichiometric interaction between gold ions and DES molecules (eq. (5)). Control experiments demonstrated that toluene alone does not extract Au^{3+}, underscoring the critical role of DEBA-Thy in the extraction process. This stoichiometric relationship confirms that DEBA-Thy components actively complex with gold ions in the toluene phase, driving the selective extraction.

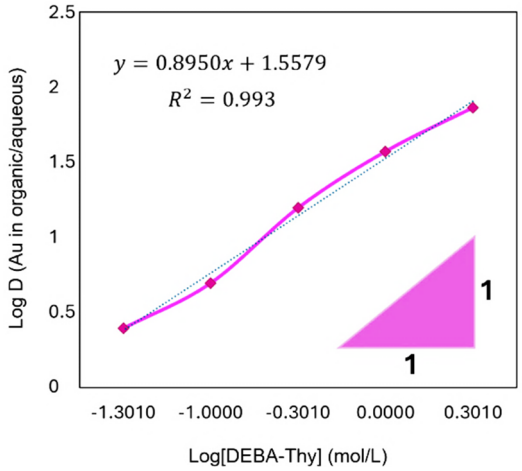

Figure 10. Slope analysis for extraction of [Au^{3+}] = 150 ppm under using DEBA-Thy under various concentrations at an initial pH of 5 with H_2SO_4 for 2 h, T = 298.15 K with an O/A ratio of 1:5.

3.6 Cytotoxicity profiles

In the pursuit of environmentally sustainable methods for gold extraction, DESs have emerged as promising alternatives to conventional solvents. The cytotoxicity of the synthesized DESs was evaluated by determining their EC_{50} values, which were found to be 72.09, 51.66, and 33.02 µmol/L for DEBA-Thy, Lid-Van, and AChCl-DEA, respectively (Figure 11). To assess their biocompatibility, these EC_{50} or IC_{50} values were compared with those of previously reported DESs and conventional extractants using the HEK-293 human cell line, as summarized in Table 5. The higher IC_{50} values observed for the prepared DESs indicate their lower cytotoxic potential, suggesting that these formulations could be safer for humans and animals.

Among the solvents tested, DEBA-Thy exhibited the highest EC_{50} value, indicating the lowest cytotoxicity and thus the greatest biocompatibility. This finding underscores its strong potential for environmentally conscious gold extraction applications. By comparison, choline chloride–ethylene glycol, a DES previously employed in gold extraction, showed moderate cytotoxicity with an EC_{50} of 62.71 µmol/L.

However, those studies often involved the use of toxic co-solvents, such as copper(II) chloride dihydrate and Aliquat 336, to enhance extraction efficiency. These co-solvents exhibited substantially lower EC_{50} values of 0.022 and 2.60 μmol/L, respectively, reflecting their significantly higher toxicity.

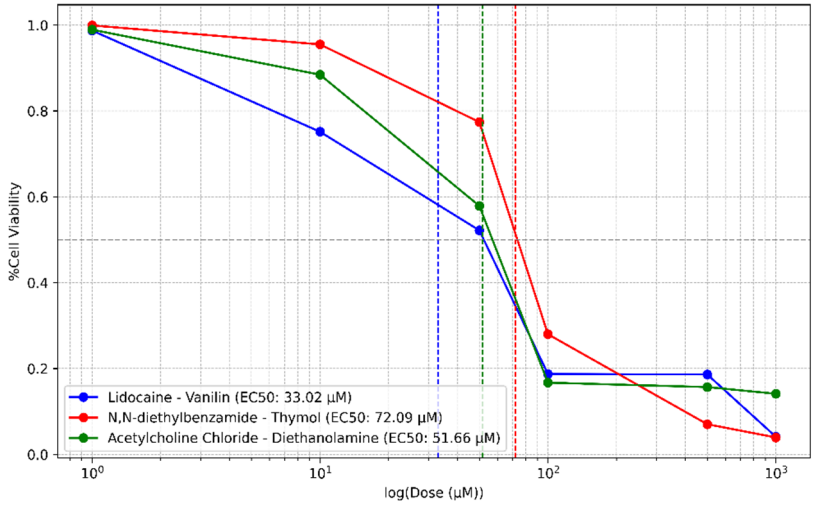

Figure 11. Dose-response curves for cytotoxicity assays of selected DES. The dashed vertical lines indicate EC_{50} values, representing the concentration at which cell viability is reduced by 50%.

Table 5. Comparison of EC_{50}/IC_{50} values for the present DESs and other solvents.

Solvent	EC_{50} /IC_{50} (μmol/L)	Ref
Choline Chloride-Raffinose	3.52	[22]
Choline Chloride-Glucosamine	4.51	[22]
Choline Chloride-Mannose	8.23	[22]
Choline Chloride-Sorbitol	11.76	[22]
Choline Chloride-Xylose	13.07	[22]
Choline Chloride-Ethyleneglycol	62.71	[22]
Copper(II) Chloride Dihydrate	0.022	[45]
Aliquat 336	2.6	[17]
Cyphos 104	0.9	[17]
Lid-Van	33.02	This study
DEBA-Thy	72.09	This study
AChCl-DEA	51.66	This study

4. Conclusion

In this study, which builds on our previous screening of DES candidates, DEBA-Thy was identified as a promising solvent based on COSMO-RS predictions of SLE phase diagrams, then validated by experimental results. Predictive modelling demonstrated high accuracy and strong agreement with

experimental data, highlighting its reliability in DES design and performance evaluation. DEBA-Thy remained stable in the liquid phase at room temperature and exhibited excellent gold extraction efficiency, while the extraction of Pd^{2+} and Pt^{4+} remained minimal under the same conditions. Furthermore, DEBA-Thy exhibited low cytotoxicity, supporting its potential as a highly promising green solvent system for the efficient and sustainable recovery of gold from complex mixtures.

Acknowledgment

This study was supported by CREST (Grant ID JPMJCR24S2) from Japan Science and Technology Agency (JST) and the Environment Research and Technology Development Fund (Grant No. JPMEERF2023002) from the Ministry of the Environment of Japan. Z.D.N. gratefully acknowledges the Ministry of Education, Culture, Sports, Science and Technology (MEXT) of Japan for the scholarship support. We also sincerely thank Diah Anggraini Wulandari and Tanabe Eri from the Department of Applied Chemistry, Graduate School of Engineering, Kyushu University, for their valuable assistance; Diah Anggraini Wulandari conducted the cytotoxicity assays of the selected DESs, and Tanabe Eri supported the metal extraction analysis.

Declaration

The authors declare no competing financial interest.

References

1) J. C. Warner, A. S. Cannon, K. M. Dye, *Environ. Impact Assess. Rev.*, **24**, 775-799 (2004).
2) P. Pollet, E. A. Davey, E. E. Ureña-Benavides, C. A. Eckert, C. L. Liotta, *Green Chem.*, **16**, 1034-1055 (2014).
3) O. S. Hammond, D. T. Bowron, K. J. Edler, *Angew. Chem. Int. Ed.*, **56**, 9782-9785 (2017).
4) R. A. Sheldon, *Green Chem.*, **7**, 267-278 (2005).
5) M. A. R. Martins, S. P. Pinho, J. A. P. Coutinho, *J. Solution Chem.*, **48**, 962-982 (2019).
6) A. P. Abbott, G. Capper, D. L. Davies, R. K. Rasheed, V. Tambyrajah, *Chem. Commun.*, 70-71 (2003).
7) Z. Huang, C. Ye, L. Li, X. Zhang, T. Qiu, *Braz. J. Chem. Eng.*, **33**, 897-906 (2016).
8) S. Seo, G. S. Lee, H. R. Kim, J.-G. Kim, *Metals*, **11**, 1785 (12 pages) (2021).
9) S. Yu, J. Zhang, S. Li, Z. Chen, Y. Wang, *Separations*, **10**, 264 (30 pages) (2023).
10) T. Lemaoui, F. A. Hatab, A. S. Darwish, A. Attoui, N. E. H. Hammoudi, G. Almustafa, M. Benaicha, Y. Benguerba, I. M. Alnashef, *ACS Sustainable Chem. Eng.*, **9**, 5783-5808 (2021).
11) S. Suffia, D. Dutta, *J. Mol. Liq.*, **394**, 123738 (17 pages) (2024).
12) S. Khandelwal, Y. K. Tailor, M. Kumar, *J. Mol. Liq.*, **215**, 345-386 (2016).
13) C. Wang, X. Lu, R. Deng, M. Guo, M. Gao, J. Ru, C. Xu, Y. Hua, Q. Zhang, *Sep. Purif. Technol.*, **364**, 132341 (16 pages) (2025).
14) M. J. Khuduwe, A. Shemi, S. Ndlovu, *Minerals*, **14**, 1239 (14 pages) (2024).
15) P. Cen, K. Spahiu, M. S. Tyumentsev, M. R. St. J. Foreman, *Phys. Chem. Chem. Phys.*, **22**, 11012-11024 (2020).
16) R. Wang, G. Fan, C. Zhang, *Waste Manag.*, **178**, 351-361 (2024).

17) A. Maghfirah, T. Hanada, A. T. N. Fajar, M. Goto, *ACS Sustainable Chem. Eng.*, **12**, 6797-6805 (2024).
18) I. Wazeer, M. Hayyan, M. K. Hadj-Kali, *J. Chem. Technol. Biotechnol.*, **93**, 945-958 (2018).
19) D. J. G. P. van Osch, C. H. J. T. Dietz, J. van Spronsen, M. C. Kroon, F. Gallucci, M. van Sint Annaland, R. Tuinier, *ACS Sustainable Chem. Eng.*, **7**, 2933-2942 (2019).
20) K. Wang, D. Peng, A. Alhadid, M. Minceva, *Ind. Eng. Chem. Res.*, **63**, 11110-11120 (2024).
21) A. Atashnezhad, J. Scott, M. F. Al Dushaishi, *ACS Sustainable Chem. Eng.*, **12**, 14684-14693 (2024).
22) R. Ahmadi, B. Hemmateenejad, A. Safavi, Z. Shojaeifard, M. Mohabbati, O. Firuzi, *Chemosphere*, **209**, 831-838 (2018).
23) A. Klamt, *Ind. Eng. Chem. Res.*, **53**, 8935 (1 page) (2014).
24) F. Eckert, A. Klamt, *AIChE J.*, **48**, 369-385 (2002).
25) A. D. Becke, *Phys. Rev. A*, **38**, 3098-3100 (1988).
26) J. P. Perdew, *Phys. Rev. B*, **33**, 8822-8824 (1986).
27) T. Hanada, M. Goto, *ACS Sustainable Chem. Eng.*, **9**, 2152-2160 (2021).
28) Y. Shen, *J. Power Sources*, **528**, 231220 (17 pages) (2022).
29) J. K. U. Ling, K. Hadinoto, *Int. J. Mol. Sci.*, **23**, 3381 (28 pages) (2022).
30) R. Hoffman, *J. Magn. Reson.*, **335**, 107105 (9 pages) (2022).
31) H. Mo, D. Raftery, *Anal. Chem.*, **80**, 9835-9839 (2008).
32) R. B. Nazarski, *Molecules*, **28**, 4369 (23 pages) (2023).
33) I. J. Ferreira, F. Oliveira, A. R. Jesus, A. Paiva, A. R. C. Duarte, *J. Mol. Liq.*, **362**, 119675 (23 pages) (2022).
34) J. L. Sebaugh, *Pharm. Stat.*, **10**, 128-134 (2011).
35) D. J. G. P. van Osch, C. H. J. T. Dietz, S. E. E. Warrag, M. C. Kroon, *ACS Sustainable Chem. Eng.*, **8**, 10591-10612 (2020).
36) M. I. Martín, I. García-Díaz, F. A. López, *Miner. Eng.*, **203**, 108306 (28 pages) (2023).
37) T. R. Sekharan, R. M. Chandira, S. C. Rajesh, S. Tamilvanan, CT. Vijayakumar, B. S. Venkateswarlu, *Biointerface Res. Appl. Chem.*, **11**, 14620-14633 (2021).
38) D. Peng, Z. Yu, A. Alhadid, M. Minceva, *Ind. Eng. Chem. Res.*, **63**, 1623-1633 (2024).
39) Y. A. Bhadange, J. Carpenter, V. K. Saharan, *ACS Omega*, **9**, 31274-31297 (2024).
40) E. Kayahan, U. D. Caprio, A. V. den Bogaert, M. N. Khan, M. Bulut, L. Braeken, T. V. Gerven, M. E. Leblebici, *Chem. Eng. Process.*, **184**, 109285 (16 pages) (2023).
41) O. S. I. Fayomi, A. P. I. Popoola, *J. Phys.: Conf. Ser.*, **1378**, 022006 (8 pages) (2019).
42) R. Liu, J. Li, X. Liu, X. Yin, Y. Yang, *Hydrometallurgy*, **226**, 106312 (9 pages) (2024).
43) R. Liu, J. Hao, Y. Wang, Y. Meng, Y. Yang, *J. Mol. Liq.*, **365**, 120200 (11 pages) (2022).